Volume 8 | Number 6 | June 2017 | Pages 4139–4668

Chemical Science

rsc.li/chemical-science

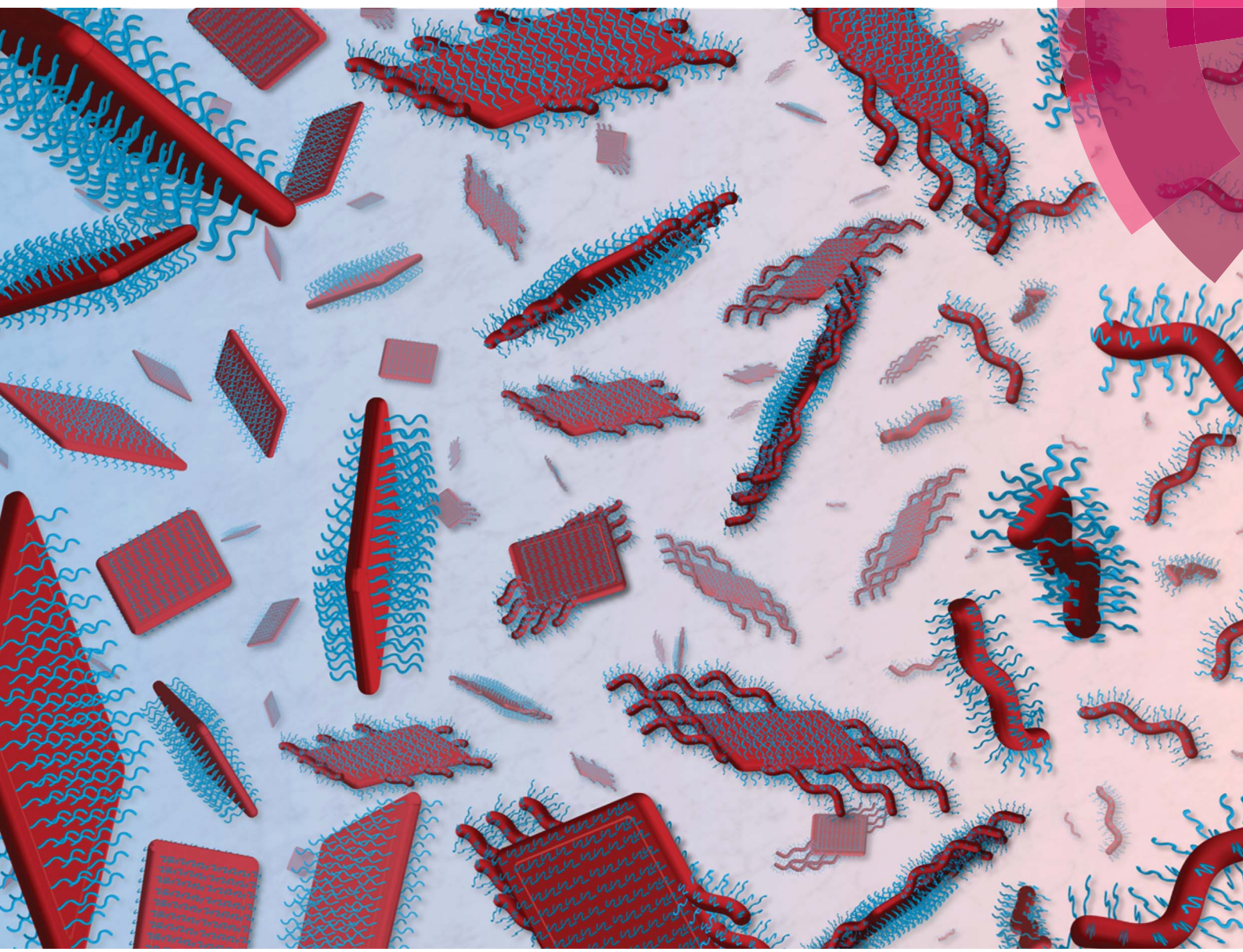

ISSN 2041-6539

ROYAL SOCIETY OF CHEMISTRY

EDGE ARTICLE

Andrew P. Dove, Rachel K. O'Reilly *et al.*

1D *vs.* 2D shape selectivity in the crystallization-driven self-assembly of polylactide block copolymers

Chemical Science

EDGE ARTICLE

View Article Online
View Journal | View Issue

Cite this: *Chem. Sci.*, 2017, **8**, 4223

1D *vs.* 2D shape selectivity in the crystallization-driven self-assembly of polylactide block copolymers†

Maria Inam,[a] Graeme Cambridge,[a] Anaïs Pitto-Barry,[a] Zachary P. L. Laker,[b] Neil R. Wilson,[b] Robert T. Mathers,[c] Andrew P. Dove *[a] and Rachel K. O'Reilly *[a]

2D materials such as graphene, LAPONITE® clays or molybdenum disulfide nanosheets are of extremely high interest to the materials community as a result of their high surface area and controllable surface properties. While several methods to access 2D inorganic materials are known, the investigation of 2D organic nanomaterials is less well developed on account of the lack of ready synthetic accessibility. Crystallization-driven self-assembly (CDSA) has become a powerful method to access a wide range of complex but precisely-defined nanostructures. The preparation of 2D structures, however, particularly those aimed towards biomedical applications, is limited, with few offering biocompatible and biodegradable characteristics as well as control over self-assembly in two dimensions. Herein, in contrast to conventional self-assembly rules, we show that the solubility of polylactide (PLLA)-based amphiphiles in alcohols results in unprecedented shape selectivity based on unimer solubility. We use log P_{oct} analysis to drive solvent selection for the formation of large uniform 2D diamond-shaped platelets, up to several microns in size, using long, soluble coronal blocks. By contrast, less soluble PLLA-containing block copolymers yield cylindrical micelles and mixed morphologies. The methods developed in this work provide a simple and consistently reproducible protocol for the preparation of well-defined 2D organic nanomaterials, whose size and morphology are expected to facilitate potential applications in drug delivery, tissue engineering and in nanocomposites.

Received 10th February 2017
Accepted 24th March 2017

DOI: 10.1039/c7sc00641a

rsc.li/chemical-science

Introduction

Conventional solution self-assembly occurs when a block copolymer is dissolved in a solvent that is selective for one of the blocks or occurs during polymerization in a selective solvent for one of the blocks.[1–3] Self-assembly is driven by a balancing of energies associated with solvation of the corona and chain packing of the core block and their relative ratio often determines the resultant micellar morphology.[3] A wide range of morphologies are accessible using this methodology, however access to free-standing sheet formation (*i.e.* 2D materials with a high aspect ratio) is often challenging, with limited examples in the literature,[4–7] due to the prevalence of the formation of closed structures such as vesicles and cylinders. Yet, free-standing sheet formation is often seen in inorganic materials assemblies such as nanosheets of molybdenum disulfide, boron nitride and LAPONITE® clays. Indeed, the discovery of graphene as a 2D material analogy of 1D carbon nanotubes has provided unheralded interest from the materials community. Such 2D high aspect materials are important as additives in composites,[8–10] thermosets[11] and as a platform for nanoparticles.[12–15]

Crystallization-driven self-assembly (CDSA) is a novel tool in the solution polymer self-assembly toolbox and has been utilized to create an impressive range of hierarchical block copolymer structures.[16] Unlike in conventional solution self-assembly, where the range of morphologies obtained are determined by varying the relative block composition of each block, polymers assembled *via* CDSA favor the formation of micelles with low interfacial curvature. Winnik and Manners have utilized the CDSA of poly(ferrocenyldimethylsilane) (PFS) block copolymers for the preparation of a wide range of high aspect nanostructures including cylinders[17–20] and platelet micelles.[21–24] However, despite these advances there are relatively few examples where the aggregate morphology can be readily controlled to form nanostructures whose size can be controlled in two dimensions.[14,25–30] Indeed, this was reported by Winnik and Manners through the utilization of CDSA to afford 2D platelet assemblies, which could be extended to grow

[a]*Department of Chemistry, University of Warwick, Gibbet Hill, Coventry, CV4 7AL, UK. E-mail: a.p.dove@warwick.ac.uk; r.k.o-reilly@warwick.ac.uk*
[b]*Department of Physics, University of Warwick, Gibbet Hill, Coventry, CV4 7AL, UK*
[c]*Department of Chemistry, Pennsylvania State University, New Kensington, Pennsylvania 15068, USA*

† Electronic supplementary information (ESI) available: Further polymer and nanostructure characterisation. See DOI: 10.1039/c7sc00641a

in 2D to form micron-sized lenticular micelles of complex function and form.[31] In these studies, it was shown that lamellae/platelets were obtained for block copolymers that have equivalent corona–core degrees of polymerization, while an increase in the degree of polymerization of the corona-forming block led to cylindrical morphologies.[24] This phenomenon was observed even when the corona-forming block was much larger than the core-forming block (20 : 1 block ratio).[32] A further report by Chen and coworkers, utilized similar block ratios with a poly(ε-caprolactone) crystalline segment to afford elongated polymer platelets with hexagonal edges.[14]

The only other report of the formation of such high aspect ratio nanostructures using CDSA was by Eisenberg, who highlighted the utilization of CDSA and homopolymer co-assembly techniques (based on a poly(ε-caprolactone) core-forming block) to allow for the formation of 2D block copolymer 'rafts'.[33,34] This approach utilized the hierarchical growth of lamellae from one dimensional rods and demonstrated the first example of the formation of highly elongated subunits (aspect ratio > 50) through spontaneous alignment without the presence of a foreign interface. This evolution of dimensionality from 1D to 2D structures was attributed to the added PCL homopolymer which was acting as a structure-driving agent.

Our group has pioneered research in the area of CDSA of amphiphilic poly(L-lactide) (PLLA)-based block copolymers.[35–37] PLLA is a biocompatible semi-crystalline polymer as well as being derived from renewable resources and has found extensive use in delivery applications.[38] Previously, we have shown that CDSA is possible for various PLLA-containing block copolymers such as *N*,*N*-dimethylacrylamide, ethylene glycol or 4-acryloyl morpholine.[39] To date, we have focused on the self-assembly of polyacrylic acid containing copolymers, PAA-*b*-PLLA, polymerized *via* ring opening polymerization (ROP) and reversible addition–fragmentation chain transfer (RAFT) polymerization, where cylindrical morphologies have been obtained with varying block compositions.[39,40] It is clear however, that CDSA rules cannot be easily generalized and translated between different polymers, and hence requires optimization of solvent systems and assembly conditions to promote the process efficiently for each system.

There is also interest in using CDSA to develop fully biocompatible and degradable high aspect ratio nanostructures for utilization in nanomedicine applications.[41] For example, Chen and coworkers showed that poly(ethylene oxide)-*b*-poly(ε-caprolactone) leaf-like sheets showed a selective internalization to different cells.[27] A number of reports also indicate that elongated morphologies clearly outperform their spherical analogues in terms of escape from phagocytosis and firm binding to the target tissue.[42,43] For example, DeSimone used a series of nanoparticles of the same shape but with differing aspect ratios to demonstrate (using particle replication in non-wetting templates technique) different levels of cellular uptake; specifically, those of higher aspect ratio showed faster uptake kinetics.[44] Indeed, it has been reported that particle shape (specifically the local particle shape at the point of initial contact) and not size plays a dominant role in phagocytosis and intracellular transport.[45–47]

In this work we use, for the first time, polymer hydrophobicity calculations from log P_{oct} analysis techniques to direct the formation of 2D nanostructures *via* CDSA in a single component solution-phase protocol. In sharp contrast to previous reports, platelets were observed for block copolymers with large corona–core block ratios (without the presence of homopolymers), while cylindrical structures were observed for smaller corona–core block ratios. We have also been able to demonstrate a novel blending methodology to allow for access to more complex 2D nanostructures. This methodology provides hitherto unprecedented access to well-defined 2D organic nanomaterials, which are difficult to access using traditional assembly methods and are expected to have potential as biocompatible nanomaterials for application as components in biomaterials and/or delivery applications.

Results and discussion

Diblock copolymers were synthesized using a previously reported method (Scheme 1, Table 1).[35] ROP of L-lactide yielded a PLLA macroinitiator, and subsequent RAFT polymerization of *N*,*N*-dimethylacrylamide (DMA) was used to prepare the corona block. SEC analysis revealed monomodal polymers with relatively low dispersities ($Đ_M$) and the absence of PLLA homopolymer as confirmed by DOSY NMR analysis (Fig. S1 and S2†).

Directing self-assembly conditions using log P_{oct} analysis

In order to select the most appropriate solvent for self-assembly, we investigated the effects of polymer solubility on nanostructure formation, where we sought to define a single, alcoholic solvent that could be selective for the corona block. As such, a series of molecular hexameric models of PLLA and PDMA were constructed, where the average amount of hydrophobicity was determined for each block and compared to the hydrophobicity of various alcoholic solvents. To quantify hydrophobicity, octanol–water partition coefficients (log P_{oct}) were calculated and normalized by surface area (SA) (Fig. 1). Previously, log P_{oct} values have provided a convenient method to quantify the hydrophobicity of monomers,[48] homopolymers and copolymers,[49] and crosslinked networks.[50] As such, we theorized that they could also

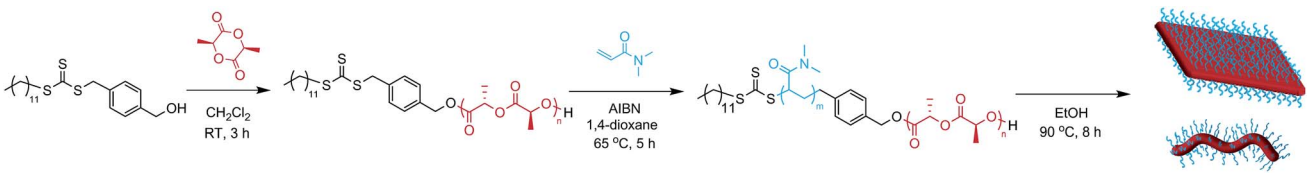

Scheme 1 Synthesis of PDMA-*b*-PLLA cylinders and diamond-shaped platelets.

Table 1 Characterization of block copolymers $PDMA_n$-b-$PLLA_m$

	M_n[a] (kg mol^{-1})	$Đ_M$[a]	$m : n$[b]	Hydrophobic wt%[c]
$PDMA_{1000}$-b-$PLLA_{48}$	122.2	1.10	20 : 1	6.9
$PDMA_{600}$-b-$PLLA_{48}$	74.1	1.06	12.5 : 1	11.0
$PDMA_{250}$-b-$PLLA_{48}$	41.5	1.05	5 : 1	22.8
$PDMA_{150}$-b-$PLLA_{48}$	28.2	1.05	3 : 1	33.0
$PDMA_{250}$-b-$PLLA_{25}$	36.3	1.17	10 : 1	13.9
$PDMA_{130}$-b-$PLLA_{25}$	25.0	1.10	5 : 1	23.7

[a] Apparent values based on SEC measurements. [b] Ratio of degrees of polymerization calculated from ^{1}H NMR integration. [c] Weight percentages calculated from ^{1}H NMR integration. Note that all PLLA wt% values lie within the previously identified region to undergo CDSA processes which yield cylindrical micelles.[40]

be used to provide a simple and reliable tool for the prediction of solvents for block copolymer self-assembly based on solubility. Compared to assessing hydrophobicity with Hildebrand solubility parameters, log P_{oct}/SA values enable faster assessment time and provide a physical meaning that can be experimentally verified. For instance, log P_{oct}/SA values for homopolymers and copolymers correlate to contact angle measurements, swelling experiments, and Nile red absorbances.[51] These calculations demonstrate that the hydrophobicity of the polymer can be correlated to the optimal hydrophobicity of the solvent in order to promote unimer solubility and allow access to well-defined constructs. Interestingly, the calculated log P_{oct} values revealed that ethanol more closely resembled the hydrophobicity of PDMA compared to *n*-propanol, *n*-butanol, and methanol. This is in contrast to predictions made using the Hildebrand system, where the solubility parameters of PDMA (25.4) and the alcohols used (ethanol (26.5), *n*-propanol (24.6), and *n*-butanol (23.2))[52] predict that *n*-propanol would be the optimum solvent for PDMA.

The results from the log P_{oct} analysis of our polymers were initially tested by investigating the self-assembly of $PDMA_{600}$-b-$PLLA_{48}$ (block ratio 12.5 : 1) in a range of alcoholic solvents. Assembly was performed in ethanol, *n*-propanol and *n*-butanol at 65 °C for 18 h followed by slow cooling to room temperature (analogous to the conditions used in our previous CDSA studies).[35] Consistent with log P_{oct} analysis, TEM imaging revealed that more well-defined 2D platelets and faceted lamellae were obtained from ethanol, whereas elongated or ill-defined structures were observed in *n*-propanol and *n*-butanol (Fig. 1). This confirmed ethanol as the optimum solvent for use in further investigations of well-defined 2D nanostructures and highlights the potential utility of log P_{oct} as an indicator of solubility parameters for self-assembly.

Optimizing the conditions for self-assembly

In order to enhance 2D particle formation, we theorised that increasing unimer solubility would reduce the dispersity of the assemblies. Our initial investigations into alternative solvents using log P_{oct} analysis demonstrated a poorer solubility with *n*-propanol and *n*-butanol, as shown previously, and methanol was found to fully solubilise the unimers (thus no structures were formed). Hence, we investigated the effect of elevated temperature and prolonged heating in ethanol to increase the solubility of the unimers prior to assembly. Indeed, at longer heating times, kinetic studies at 90 °C revealed increasingly well-defined diamond platelets (Fig. 2a) for the largest corona–core ratio (20 : 1) of up to 10 μm in length and *ca.* 15 nm thick (Fig. 2d and S4†), where 8 h was determined to be the optimum time required to achieve consistently reproducible smooth diamond-shaped platelets. These structures are similar to those observed for PLLA single crystals where "lozenge" shaped crystals are reported.[53,54] The concentration dependent assembly of the diamond platelets showed no discernible change in morphology, particle dispersity or size at concentrations up to 25 mg mL^{-1}. Notably, all of the observed diamonds were consistently larger than those formed at 65 °C due to the elevated dissolution temperatures reducing the number of crystalline nuclei, thus producing a smaller number of larger structures. Indeed, extending the heating time further resulted in more platelet structures, even for the smaller corona–core ratios (Fig. S5†).

Exploring the effect of polymer composition on self-assembly

To further expand the scope of our investigation and determine how the solubility of the coronal block in ethanol affects the self-assembly process, a range of PDMA : PLLA block ratios were

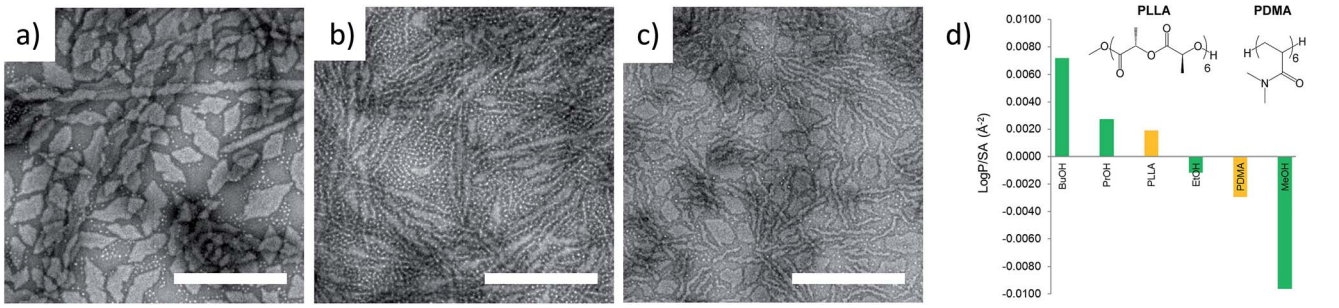

Fig. 1 TEM micrographs of corona–core ratio 12.5 : 1 $PDMA_{600}$-b-$PLLA_{48}$ self-assembled in (a) ethanol, (b) *n*-propanol and (c) *n*-butanol at 65 °C for 18 h and cooled to room temperature. All samples were stained with uranyl acetate. Scale bar = 1 μm. (d) Structure of hexameric models based on polylactide (PLLA) and poly(*N*,*N*-dimethylacrylamide) (PDMA) and log P_{oct} hydrophobicity calculations compared to methanol (MeOH), ethanol (EtOH), propanol (PrOH), and butanol (BuOH). A similar trend was noted with oligomeric models composed of octamers. PLLA incorporated a MeO initiator with an OH endgroup. PDMA was hydrogen terminated (see Fig. S3†).

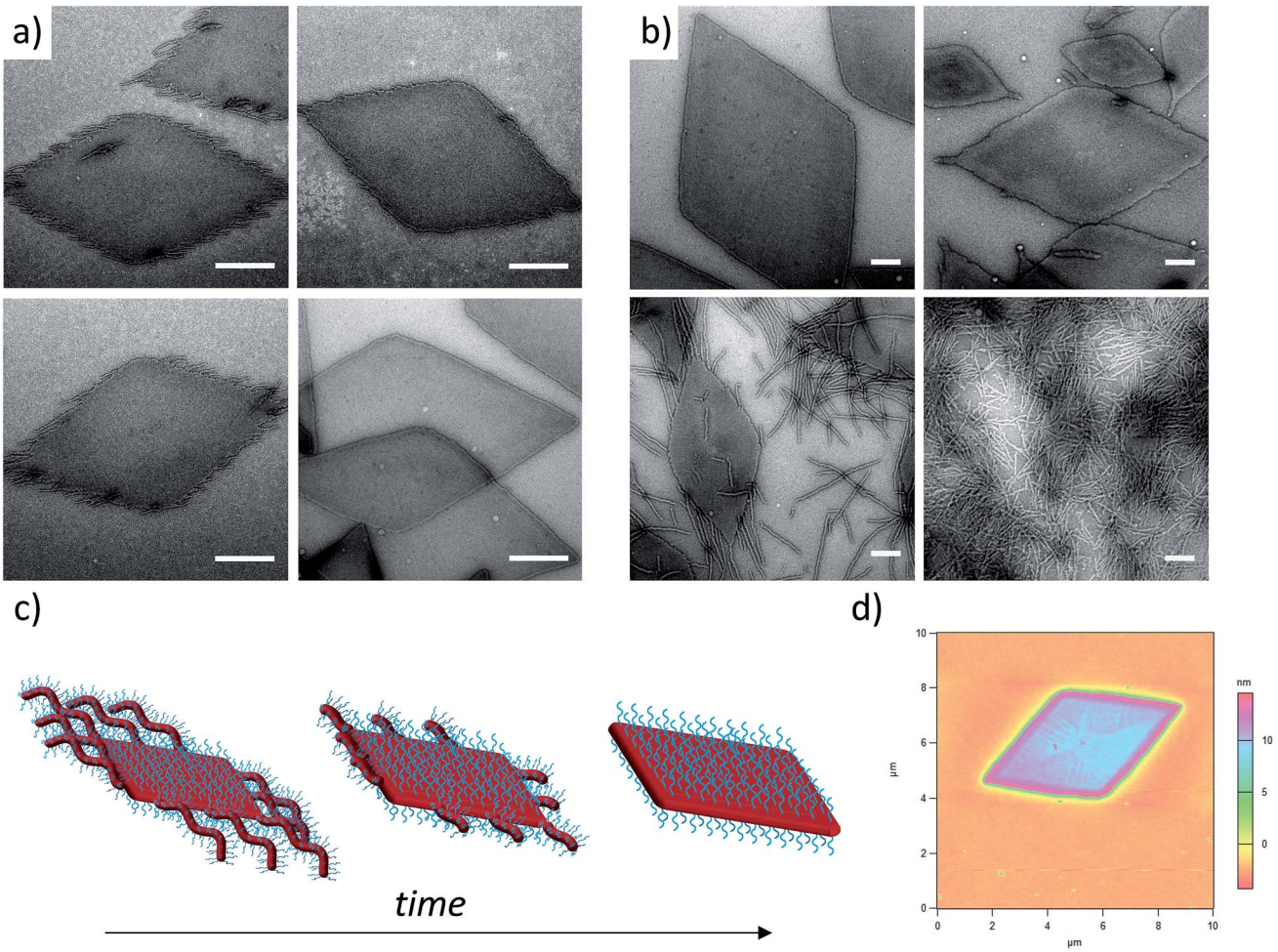

Fig. 2 (a) TEM micrographs of corona–core ratio 20 : 1 $PDMA_{1000}$-*b*-$PLLA_{48}$ self-assembled in ethanol at 90 °C for 2 h (top left), 4 h (top right), 6 h (bottom left) and 8 h (bottom right) before cooling to room temperature. (b) TEM micrographs of a series of $PDMA_m$-*b*-$PLLA_{48}$ block copolymers of corona–core ratios of 20 : 1 (m = 1000, top left), 12.5 : 1 (m = 600, top right), 5 : 1 (m = 250, bottom left), and 3 : 1 (m = 150, bottom right). Samples were self-assembled in ethanol at 90 °C for 8 h and cooled to room temperature. All samples were stained with uranyl acetate. Scale bar = 1 μm. (c) Schematic of diamond platelet formation kinetics. (d) AFM of diamond platelet assembled from 20 : 1 corona–core ratio diblock copolymer.

synthesized (Table 1). Decreasing the PDMA block length to give 12.5 : 1 and 5 : 1 block ratios (using a $PLLA_{48}$ core block) resulted in mixed phases of structures primarily diamond in shape, with clear dispersity in size, and evidence of elongated ends and cylindrical micelles (Fig. 2b). In comparison, purely cylindrical structures were obtained from the lowest PDMA block length (3 : 1), which suggests that under these conditions, the crossover composition[31] has been reached in this system. Similar observations (Fig. S6†) were made during the assembly of a second PLLA block which had a lower DP ($PDMA_{250}$-*b*-$PLLA_{25}$) but was more similar to the PLLA block lengths previously reported by our groups (where no evidence of 2D structures was observed).[40] These observations are in stark contrast to the widely reported PFS system, where elongated structures are formed when the corona-forming block is much larger than the core-forming block[24] to accommodate the large volume occupied by the corona chains.[55]

Characterization of the assemblies

To further investigate the dimensions of specific 2D diamond-shaped nanostructures in solution, small angle X-ray scattering (SAXS) analysis was performed.[56] It has been demonstrated that at intermediate q values, the scattering intensity $I(q)$ is proportional to q^{-D} with D being the fractal exponent of the scattering objects, where dispersed plate-like objects have a D value of 2 while aggregates or folded structures have typical D values between 3 and 4.[57] Upon examination, the 20 : 1 corona–core ratio platelets (Fig. 2a) exhibit a slope of −2 for intermediate q values (Fig. S7a†), which confirms the presence of one-dimensional objects as observed by TEM. The early stage of a plateau is observable at low q values,[58] with a repeat distance which correlates closely with the platelet sizes observed by TEM analysis. The slope observed at low q values is close to −3, which suggests that some plates may have stacked together during analysis. The Guinier plot (Fig. S7b†) for flat particles allows the determination of the thickness τ from the slope R_τ^2 of the linear

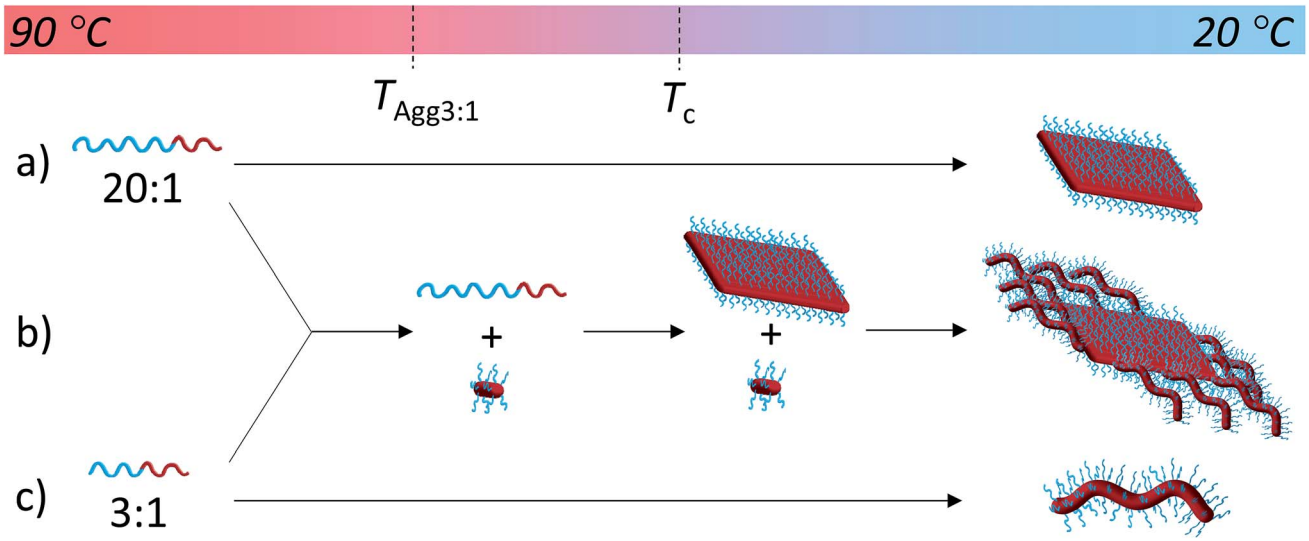

Scheme 2 Solvation-driven shape selectivity mechanism (using an arbitrary scale to represent sequential processes on cooling from 90 °C to 20 °C) for $PDMA_m$-*b*-$PLLA_{48}$ block copolymers of block ratios (a) 20 : 1 (platelet-forming, $m = 1000$); (b) a mixture of 20 : 1 and 3 : 1 and (c) 3 : 1 (cylinder-forming, $m = 150$), where $T_{Agg3:1}$ represents aggregation of the 3 : 1 block ratio cylinder-forming block copolymer.

region with the following equation: $\tau^2 = 12 \times R_\tau^2$ with R_τ being the one-dimensional radius of gyration taken from the center of the platelet perpendicular to the face.[59] A thickness just below 2 nm is found for the 20 : 1 corona–core ratio $PDMA_{1000}$-*b*-$PLLA_{48}$ platelets. It is expected this thickness mainly relates to the crystalline block as the scattering length density contrast between the solvent and the two blocks is much higher for the crystallized polylactide block than for the amorphous and solvated DMA block.

Selected area electron diffraction (SAED) was also performed on the diamond platelets, formed from the 20 : 1 corona–core ratio diblock copolymer, which confirmed the crystalline nature of the diamonds (Fig. S8†) in addition to wide-angle X-ray scattering (WAXS) analysis (Fig. S9†). The SAED patterns are consistent with the orthorhombic unit cell previously reported for PLLA (with reciprocal lattice parameters; $\alpha^* = 0.935\ nm^{-1}$, $\beta^* = 1.626\ nm^{-1}$, $\gamma^* = 90°$)[44] and, along with the diamond shape of the platelets, indicate the {110} growth plane. Furthermore, taking into consideration the fiber repeat distance and molecular weights, we propose that the chain-folding occurs at lamellar surfaces of single crystals. The highly crystalline nature of the assembly also suggests the PLLA component crystallizes in a structure essentially identical to that expected for PLLA on its own.[54] Although various confined crystal micelles in selective solvents for the amorphous block have been investigated extensively, the formation of well-defined block copolymer crystals is rarely reported.[24,26,60–64]

Understanding the assembly process

Unlike other systems that utilize CDSA, which rely on solvent quality for the core-forming block,[21] the formation of these fibers and 2D nanostructures appears to be governed by the

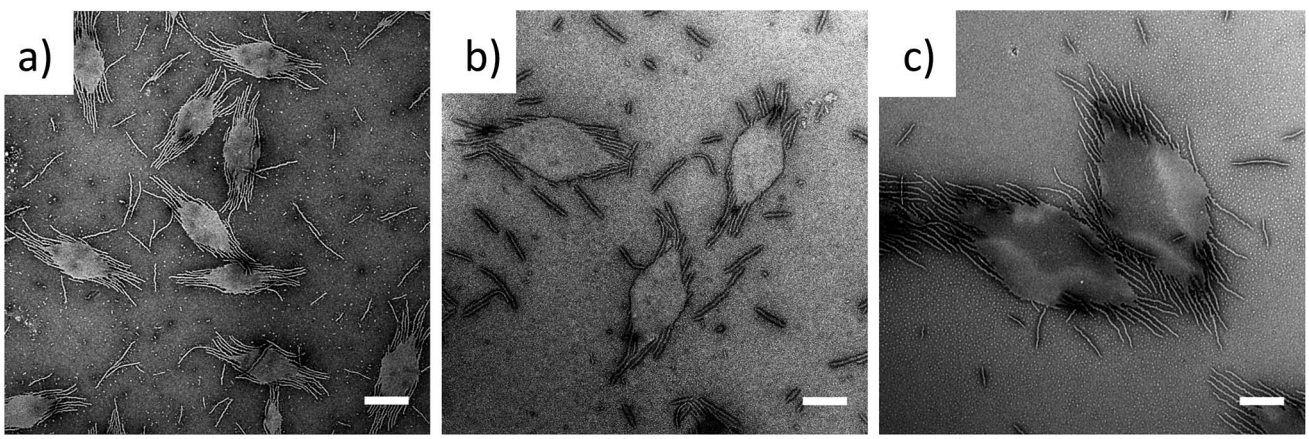

Fig. 3 TEM micrographs of $PDMA_m$-*b*-$PLLA_{48}$ blends of block ratios 20 : 1 ($m = 1000$) and 3 : 1 ($m = 150$), at blending ratios of (a) 25 : 75, (b) 50 : 50 and (c) 75 : 25, self-assembled in ethanol at 90 °C for 8 h and cooled to room temperature. Samples were stained with uranyl acetate. Scale bar = 1 μm.

interplay between the crystallization of the PLLA core and the solubility of the corona block. On cooling, block copolymers that form unimers above the crystallization temperature of the PLLA block favor crystallization, thus reducing crystal defects and ultimately crystallizing similarly to PLLA homopolymers to form 2D diamond plates (Scheme 2a). In contrast, block copolymers that are less soluble above the crystallization temperature of the PLLA block form aggregates that undergo a crystallization event with epitaxial growth through a unimer exchange process akin to the well-established CDSA principle (Scheme 2c). To provide further evidence for this mechanism, we increased the solubility of the PDMA corona block of a cylinder-forming block copolymer (3 : 1 block ratio) by adding a single acid group to the chain end. Assembly under the same conditions resulted in a change in morphology from pure fibers towards a diamond platelet phase (Fig. S10†).

Exploring the versatility of this approach

To exploit this concept in creating complex nanostructures, and inspired by recent work in block copolymer blending,[65–68] we explored the resultant assembly of mixtures of the two block copolymer compositions (Scheme 2b, Fig. 3). We postulated that blending different ratios of platelet-forming block copolymer (20 : 1 block ratio, $PDMA_{1000}$-*b*-$PLLA_{48}$) and cylinder-forming block copolymer (3 : 1 block ratio, $PDMA_{150}$-*b*-$PLLA_{48}$) and self-assembling in ethanol for 8 h at 90 °C followed by cooling to room temperature, would lead first to assembly of the platelet-forming block copolymers which, in turn, would act as a seed for the aggregated cylinder-forming unimers to undergo epitaxial growth. Satisfyingly, the resultant assemblies did indeed exhibit a diamond center with fibers attached parallel to the long axis of the diamond. While a small number of cylinders are observed in solution (presumably from unavoidable self-nucleation events), fibers on the same side of the diamond grow unidirectionally and are quite uniform in length (Fig. S11†).

Conclusions

We have demonstrated a simple, single component solution-phase methodology that can be used as an alternative to the commonly applied surface growth approach for block copolymer single crystal preparation, greatly simplifying access to and the design of well-defined 2D organic nanomaterials. It is proposed that these advances will enable this field to fully investigate the potential for these unique and interesting materials towards mimicking the success of their inorganic analogues.

We have further simplified synthetic access to hierarchical nanostructures by demonstrating how log P_{oct} analysis can be used to predict optimal solvents for CDSA processes to avoid laborious screening methods in solvent selection, a process that could, with further study, yield significant insights into developing methods to predict solvent systems to direct CDSA. Within this, the importance of solubility in obtaining novel structures has been highlighted, where two factors that influence the solubility of the copolymer were considered; the quality of the solvent for the corona block and the ratio of block lengths. In contrast to previous reports of platelet nanoparticles,[11,69] diamond-shaped platelets were formed with good solvent quality for the corona block and large corona–core ratios, while more elongated and less defined structures were formed with poorer solvent quality and smaller block ratios. As the polymer becomes less soluble (corona chain length decreases or the solvent quality becomes worse), there is not adequate time for the PLLA chains to adopt a preferred crystal conformation thus resulting in less defined or elongated structures. We propose that the ability of the corona block to solubilize, and thus stabilize, the block copolymer in solution allows the PLLA block to crystallize to a greater extent to yield diamonds which have the appearance of defect-free plates.

Given the high interest in 2D inorganic materials, the ability to readily access and control the assembly of polymers into 2D organic platelets through a simple assembly process provides a platform to develop a range of new materials. Moreover, given their well-defined size, morphology and high stability, applications within nanocomposites, thermosets and platforms for nanoparticle delivery vehicles will be of high interest.

Acknowledgements

The authors would like to thank the University of Warwick, Materials GRP, EPSRC, The Royal Society and ERC for funding.

Notes and references

1 Y. Mai and A. Eisenberg, *Chem. Soc. Rev.*, 2012, **41**, 5969–5985.
2 N. J. Warren and S. P. Armes, *J. Am. Chem. Soc.*, 2014, **136**, 10174–10185.
3 A. Blanazs, S. P. Armes and A. J. Ryan, *Macromol. Rapid Commun.*, 2009, **30**, 267–277.
4 R. M. Van Horn, J. X. Zheng, H.-J. Sun, M.-S. Hsiao, W.-B. Zhang, X.-H. Dong, J. Xu, E. L. Thomas, B. Lotz and S. Z. Cheng, *Macromolecules*, 2010, **43**, 6113–6119.
5 P. Yang and Y. Han, *Macromol. Rapid Commun.*, 2009, **30**, 1509–1514.
6 W. Huang, C. Luo, H. Wang and Y. Han, *Polym. Int.*, 2010, **59**, 1064–1070.
7 E. D. Gomez, T. J. Rappl, V. Agarwal, A. Bose, M. Schmutz, C. M. Marques and N. P. Balsara, *Macromolecules*, 2005, **38**, 3567–3570.
8 R. M. Erb, R. Libanori, N. Rothfuchs and A. R. Studart, *Science*, 2012, **335**, 199–204.
9 L. J. Bonderer, A. R. Studart and L. J. Gauckler, *Science*, 2008, **319**, 1069–1073.
10 D. Gournis and G. Floudas, *Chem. Mater.*, 2004, **16**, 1686–1692.
11 C. Sinturel, M. Vayer, R. Erre and H. Amenitsch, *Eur. Polym. J.*, 2009, **45**, 2505–2512.
12 B. Yu, X. Jiang and J. Yin, *Chem. Commun.*, 2013, **49**, 603–605.
13 B. Li, B. Wang, R. C. Ferrier Jr and C. Y. Li, *Macromolecules*, 2009, **42**, 9394–9399.

14 J. Wang, W. Zhu, B. Peng and Y. Chen, *Polymer*, 2013, **54**, 6760–6767.
15 B. Dong, T. Zhou, H. Zhang and C. Y. Li, *ACS Nano*, 2013, **7**, 5192–5198.
16 J. J. Crassous, P. Schurtenberger, M. Ballauff and A. M. Mihut, *Polymer*, 2015, **62**, A1–A13.
17 S. K. Patra, R. Ahmed, G. R. Whittell, D. J. Lunn, E. L. Dunphy, M. A. Winnik and I. Manners, *J. Am. Chem. Soc.*, 2011, **133**, 8842–8845.
18 J. Schmelz, A. E. Schedl, C. Steinlein, I. Manners and H. Schmalz, *J. Am. Chem. Soc.*, 2012, **134**, 14217–14225.
19 X. Wang, G. Guerin, H. Wang, Y. Wang, I. Manners and M. A. Winnik, *Science*, 2007, **317**, 644–647.
20 A. Nazemi, C. E. Boott, D. J. Lunn, J. Gwyther, D. W. Hayward, R. M. Richardson, M. A. Winnik and I. Manners, *J. Am. Chem. Soc.*, 2016, **138**, 4484–4493.
21 S. F. Mohd Yusoff, M.-S. Hsiao, F. H. Schacher, M. A. Winnik and I. Manners, *Macromolecules*, 2012, **45**, 3883–3891.
22 A. Presa Soto, J. B. Gilroy, M. A. Winnik and I. Manners, *Angew. Chem., Int. Ed.*, 2010, **49**, 8220–8223.
23 G. Molev, Y. Lu, K. S. Kim, I. C. Majdalani, G. Guerin, S. Petrov, G. Walker, I. Manners and M. A. Winnik, *Macromolecules*, 2014, **47**, 2604–2615.
24 L. Cao, I. Manners and M. A. Winnik, *Macromolecules*, 2002, **35**, 8258–8260.
25 Y.-J. Kim, C.-H. Cho, K. Paek, M. Jo, M.-k. Park, N.-E. Lee, Y.-j. Kim, B. J. Kim and E. Lee, *J. Am. Chem. Soc.*, 2014, **136**, 2767–2774.
26 M. Su, H. Huang, X. Ma, Q. Wang and Z. Su, *Macromol. Rapid Commun.*, 2013, **34**, 1067–1071.
27 W. Zhu, B. Peng, J. Wang, K. Zhang, L. Liu and Y. Chen, *Macromol. Biosci.*, 2014, **14**, 1764–1770.
28 H. Qi, T. Zhou, S. Mei, X. Chen and C. Y. Li, *ACS Macro Lett.*, 2016, **5**, 651–655.
29 B. Yu, X. Jiang and J. Yin, *Macromolecules*, 2014, **47**, 4761–4768.
30 H. Qiu, Y. Gao, C. E. Boott, O. E. Gould, R. L. Harniman, M. J. Miles, S. E. Webb, M. A. Winnik and I. Manners, *Science*, 2016, **352**, 697–701.
31 Z. M. Hudson, C. E. Boott, M. E. Robinson, P. A. Rupar, M. A. Winnik and I. Manners, *Nat. Chem.*, 2014, **6**, 893–898.
32 G. Cambridge, G. Guerin, I. Manners and M. A. Winnik, *Macromol. Rapid Commun.*, 2010, **31**, 934–938.
33 G. Rizis, T. G. van de Ven and A. Eisenberg, *Angew. Chem., Int. Ed.*, 2014, **53**, 9000–9003.
34 G. Rizis, T. G. van de Ven and A. Eisenberg, *ACS Nano*, 2015, **9**, 3627–3640.
35 N. Petzetakis, A. P. Dove and R. K. O'Reilly, *Chem. Sci.*, 2011, **2**, 955–960.
36 N. Petzetakis, D. Walker, A. P. Dove and R. K. O'Reilly, *Soft Matter*, 2012, **8**, 7408–7414.
37 L. Sun, A. Pitto-Barry, N. Kirby, T. L. Schiller, A. M. Sanchez, M. A. Dyson, J. Sloan, N. R. Wilson, R. K. O'Reilly and A. P. Dove, *Nat. Commun.*, 2014, **5**, 5746–5754.
38 J. M. Becker, R. J. Pounder and A. P. Dove, *Macromol. Rapid Commun.*, 2010, **31**, 1923–1937.
39 A. Pitto-Barry, N. Kirby, A. P. Dove and R. K. O'Reilly, *Polym. Chem.*, 2014, **5**, 1427–1436.
40 L. Sun, N. Petzetakis, A. Pitto-Barry, T. L. Schiller, N. Kirby, D. J. Keddie, B. J. Boyd, R. K. O'Reilly and A. P. Dove, *Macromolecules*, 2013, **46**, 9074–9082.
41 M. Elsabahy and K. L. Wooley, *Chem. Soc. Rev.*, 2012, **41**, 2545–2561.
42 Y. Geng, P. Dalhaimer, S. Cai, R. Tsai, M. Tewari, T. Minko and D. E. Discher, *Nat. Nanotechnol.*, 2007, **2**, 249–255.
43 N. Daum, C. Tscheka, A. Neumeyer and M. Schneider, *Wiley Interdiscip. Rev.: Nanomed. Nanobiotechnol.*, 2012, **4**, 52–65.
44 S. E. Gratton, P. A. Ropp, P. D. Pohlhaus, J. C. Luft, V. J. Madden, M. E. Napier and J. M. DeSimone, *Proc. Natl. Acad. Sci. U. S. A.*, 2008, **105**, 11613–11618.
45 J. A. Champion and S. Mitragotri, *Proc. Natl. Acad. Sci. U. S. A.*, 2006, **103**, 4930–4934.
46 S. Wilhelm, A. J. Tavares, Q. Dai, S. Ohta, J. Audet, H. F. Dvorak and W. C. Chan, *Nat. Rev. Mater.*, 2016, **1**, 16014.
47 E. Hinde, K. Thammasiraphop, H. T. Duong, J. Yeow, B. Karagoz, C. Boyer, J. J. Gooding and K. Gaus, *Nat. Nanotechnol.*, 2016, **12**, 81–89.
48 D. Dakshinamoorthy, A. K. Weinstock, K. Damodaran, D. F. Iwig and R. T. Mathers, *ChemSusChem*, 2014, **7**, 2923–2929.
49 A. J. Magenau, J. A. Richards, M. A. Pasquinelli, D. A. Savin and R. T. Mathers, *Macromolecules*, 2015, **48**, 7230–7236.
50 J. Waggel and R. T. Mathers, *RSC Adv.*, 2016, **6**, 62884–62889.
51 E. Yildirim, D. Dakshinamoorthy, M. J. Peretic, M. A. Pasquinelli and R. T. Mathers, *Macromolecules*, 2016, **49**, 7868–7876.
52 J. E. Mark, *Physical Properties of Polymers Handbook*, Springer, 2007.
53 Y.-W. Chiang, Y.-Y. Hu, J.-N. Li, S.-H. Huang and S.-W. Kuo, *Macromolecules*, 2015, **48**, 8526–8533.
54 T. Iwata and Y. Doi, *Macromolecules*, 1998, **31**, 2461–2467.
55 G. Cambridge, M. J. Gonzalez-Alvarez, G. Guerin, I. Manners and M. A. Winnik, *Macromolecules*, 2015, **48**, 707–716.
56 M. J. Hollamby, *Phys. Chem. Chem. Phys.*, 2013, **15**, 10566–10579.
57 E. M. Milner, N. T. Skipper, C. A. Howard, M. S. Shaffer, D. J. Buckley, K. A. Rahnejat, P. L. Cullen, R. K. Heenan, P. Lindner and R. Schweins, *J. Am. Chem. Soc.*, 2012, **134**, 8302–8305.
58 C. Perry, P. Hébraud, V. Gernigon, C. Brochon, A. Lapp, P. Lindner and G. Schlatter, *Soft Matter*, 2011, **7**, 3502–3512.
59 E. K. Lin and A. P. Gast, *Macromolecules*, 1996, **29**, 4432–4441.
60 A. P. Gast, P. K. Vinson and K. A. Cogan-Farinas, *Macromolecules*, 1993, **26**, 1774–1776.
61 M.-S. Hsiao, J. X. Zheng, S. Leng, R. M. Van Horn, R. P. Quirk, E. L. Thomas, H.-L. Chen, B. S. Hsiao, L. Rong, B. Lotz and S. Z. Cheng, *Macromolecules*, 2008, **41**, 8114–8123.
62 M.-S. Hsiao, W. Y. Chen, J. X. Zheng, R. M. Van Horn, R. P. Quirk, D. A. Ivanov, E. L. Thomas, B. Lotz and S. Z. Cheng, *Macromolecules*, 2008, **41**, 4794–4801.

63 M.-S. Hsiao, J. X. Zheng, R. M. Van Horn, R. P. Quirk, E. L. Thomas, H.-L. Chen, B. Lotz and S. Z. Cheng, *Macromolecules*, 2009, **42**, 8343–8352.
64 J. X. Zheng, H. Xiong, W. Y. Chen, K. Lee, R. M. Van Horn, R. P. Quirk, B. Lotz, E. L. Thomas, A.-C. Shi and S. Z. D. Cheng, *Macromolecules*, 2006, **39**, 641–650.
65 D. B. Wright, J. P. Patterson, A. Pitto-Barry, A. Lu, N. Kirby, N. C. Gianneschi, C. Chassenieux, O. Colombani and R. K. O'Reilly, *Macromolecules*, 2015, **48**, 6516–6522.
66 D. B. Wright, J. P. Patterson, N. C. Gianneschi, C. Chassenieux, O. Colombani and R. K. O'Reilly, *Polym. Chem.*, 2016, **7**, 1577–1583.
67 J. Zhu, S. Zhang, K. Zhang, X. Wang, J. W. Mays, K. L. Wooley and D. J. Pochan, *Nat. Commun.*, 2013, **4**, 2294.
68 Y. Chen, K. Zhang, X. Wang, F. Zhang, J. Zhu, J. W. Mays, K. L. Wooley and D. J. Pochan, *Macromolecules*, 2015, **48**, 5621–5631.
69 T. Vilgis and A. Halperin, *Macromolecules*, 1991, **24**, 2090–2095.

Electronic Supplementary Material (ESI) for Chemical Science.

Supporting Information for

1D vs 2D shape selectivity in the crystallization-driven self-assembly of polylactide block copolymers

Maria Inam,[a] Graeme Cambridge,[a] Anaïs Pitto-Barry,[a] Zachary Laker,[b] Neil Wilson,[b] Robert T. Mathers,[c] Andrew P. Dove*,[a] and Rachel K. O'Reilly*,[a]

[a]Department of Chemistry, University of Warwick, Gibbet Hill, Coventry, CV4 7AL, United Kingdom
[b]Department of Physics, University of Warwick, Gibbet Hill, Coventry, CV4 7AL, United Kingdom
[c]Department of Chemistry, Pennsylvania State University, New Kensington, Pennsylvania 15068, United States

Materials and Methods

Materials. Chemicals and solvents were purchased from Sigma Aldrich, Acros, Fluka, Fisher Chemical, Alfa Aesar, or VWR. L-Lactide monomer was kindly donated by Corbion-Purac and dried over 3 Å molecular sieves in dichloromethane before recrystallization from toluene and stored in a glovebox with inert atmosphere. 1,4-Dioxane and *N*,*N*-dimethylacrylamide (DMA) were purified by passing through basic alumina before use. (−)-Sparteine was dried over calcium hydride and distilled before use. Bis[(trifluoromethyl)phenyl]-3-cyclohexylthiourea was prepared as previously reported.[1] 2,2'-azobis(2-methylpropionitrile), AIBN, was recrystallized twice from methanol and stored in the dark at 4 °C.

Polymer Synthesis. Poly($_L$-lactide) (PLLA) was synthesized using ring-opening polymerization (ROP) using a functional RAFT agent[2] to yield PLLA macroinitiators of varying DP.[3] Poly(*N,N*-dimethylacrylamide)-*b*-poly($_L$-lactide) (PDMA-*b*-PLLA) was synthesized by chain extending the macro PLLA initiator with *N*,*N*-dimethylacrylamide.[4]

Polymer Characterization. ^{1}H and ^{13}C NMR spectra were recorded at 400 MHz on a Bruker DPX-400 spectrometer in $CDCl_3$ unless otherwise stated. Chemical shifts are reported as δ in parts per million (ppm) downfield from the internal standard trimethylsilane.

Size exclusion chromatography (SEC) measurements in THF were performed on a Varian 390-LC-Multi detector suite fitted with differential refractive index (DRI) and photodiode array (PDA) detectors equipped with a guard column (Varian Polymer Laboratories PLGel 5 µm (50 × 7.5 mm)) and two mixed-D columns (Varian Polymer Laboratories PLGel 5 µm (300 × 7.5 mm)) using THF with 2% triethylamine eluent at a flow rate of 1.0 mL min^{-1}. SEC measurements in DMF were performed on a Varian 390-LC-Multi detector suite system fitted with RI and ultraviolet (UV) detectors (λ = 309 nm) equipped with a PLGel 3 µm (50 × 7.5 mm) guard column and two PLGel 5 µm (300 × 7.5 mm) mixed-D columns using DMF with 0.1% LiBr at 50 °C as the eluent at a flow rate of 1.0 mL min^{-1}. SEC data was calibrated against PS or PMMA standards and analyzed using Cirrus v3.3 software.

Mass spectra were obtained using a Bruker Ultraflex II Matrix-assisted laser desorption/ionisation time of flight (MALDI-ToF) mass spectrometer. Typical preparation of

samples is as follows; *trans*-2-[3-(4-*tert*-butyl-phenyl)-2-methyl-2-propenylidene] malononitrile (DCTB) matrix (20 µL of a 40 mg mL^{-1} HPLC-grade THF solution) was added to the sample (20 µL of a 1 mg mL^{-1} HPLC-grade THF solution) followed by sodium trifluoroacetate (NaTFA) (20 µL of a 0.1 mg mL^{-1} HPLC-grade THF solution) and vortexed before application on a MALDI-ToF plate. Samples were measured in reflectron ion mode and calibrated against SpheriCal (1200 – 8000 g mol^{-1}) standards.

Self-Assembly. As an example of self-assembly conditions, PDMA-*b*-PLLA (10 mg) was added to 2 mL of ethanol (5.0 mg/mL) in a 7 mL vial. The samples were heated in an oil bath at 65 °C or 90 ^{o}C, without stirring for a predetermined period of time before being removed from the oil bath and left to cool to room temperature. Samples were imaged after 1 day of ageing at room temperature.

Transmission Electron Microscopy (TEM). Samples for TEM analysis were prepared by drop casting 7 µL of polymer in ethanol (0.5 mg/mL) onto a carbon/formvar-coated copper grid placed on filter paper. Samples were stained with a 1% uranyl acetate solution to facilitate imaging of the thin organic structures unless specified. Samples were also prepared on graphene oxide support films[5] to negate the necessity for staining. Imaging for samples heated to 65 °C was performed on a Jeol 2000FX transmission electron microscope operating at 200 kV. Imaging for samples heated to 90 °C was performed on a Jeol 2100 transmission electron microscope operating at 120 kV.

Atomic Force Microscopy (AFM). Samples for AFM analysis were prepared by drop casting 7 µL of polymer in ethanol (0.25 mg/mL) onto silicon wafer followed by drying with compressed air. Imaging and analysis were performed on an Asylum Research MFP3D-SA atomic force microscope in alternate contact (tapping) mode.

Selected Area Electron Diffraction (SAED). Samples for SAED analysis were prepared by drop casting 7 µL of polymer in ethanol (0.5 mg/mL) onto a graphene oxide-coated holey Quantifoil grid placed on filter paper. Low-dose SAED was performed on a Jeol 2100 LaB6 transmission electron microscope operating at 200 kV. The diffraction spots from the graphene oxide allow direct and accurate calibration of the diffraction pattern.

Wide Angle X-ray Scattering (WAXS). WAXS was performed on a Panalytical X'Pert Pro MPD equipped with a Cu $K\alpha_1$ hybrid monochromator as the incident beam optics. Typically, *ca.* 30 mg of freeze-dried particles was placed in a 10 mm sample holder, and standard "powder" 2θ–θ diffraction scans were carried out in the angular range from 10° to 30° 2θ at room temperature. The WAXS diffractograms were processed by MDI Jade software to calculate crystallinity.

Small Angle X-ray Scattering (SAXS). SAXS measurements were recorded at the Australian Synchrotron facility at a photon energy of 12 keV and two sample-to-detector distances of 1.020 and 7.160 m to give a q range of 0.002 to 0.2 $Å^{-1}$ after merging. Q is the scattering vector and is related to the scattering angle (2θ) and the photon wavelength (λ) by $q = 4\pi\sin(\theta)/\lambda$. Samples were loaded into 1.5 mm diameter quartz capillaries that were sealed with parafilm. The capillaries were held on a temperature-controlled mount with temperature control *via* a water bath connected to a brass block which is part of the sample holder. Temperatures up to 90 °C were reached and time was allowed for samples to equilibrate. The scattering from a blank (ethanol) was measured and subtracted for each measurement and temperature and data were normalized for total transmitted flux using a quantitative beamstop detector. The two-dimensional SAXS images were converted into one-dimensional SAXS profile (*I versus q*) by circular averaging using ScatterBrain, the SAXS software developed at the Australian Synchrotron. NCNR data Analysis IGOR PRO software and Primus were used to plot and analyze SAXS data.

Computation of LogP values. After constructing hexameric oligomers (See Figure 1) to represent the hydrophobicity of the parent polymer, the oligomers were minimized with the MM2 forcefield in Chem3D Pro version 13.0.2.3021. Then, octanol-water partition coefficient ($LogP_{oct}$) were calculated with the chemical properties module. The Connolly surface area was calculated with a probe of 1.4 Å. $LogP_{oct}$ values for the diblock copolymers were calculated with Materials Studio after Forcite geometry optimization of diblock copolymers using a 1.4 Å probe for the Connolly SA calculation.

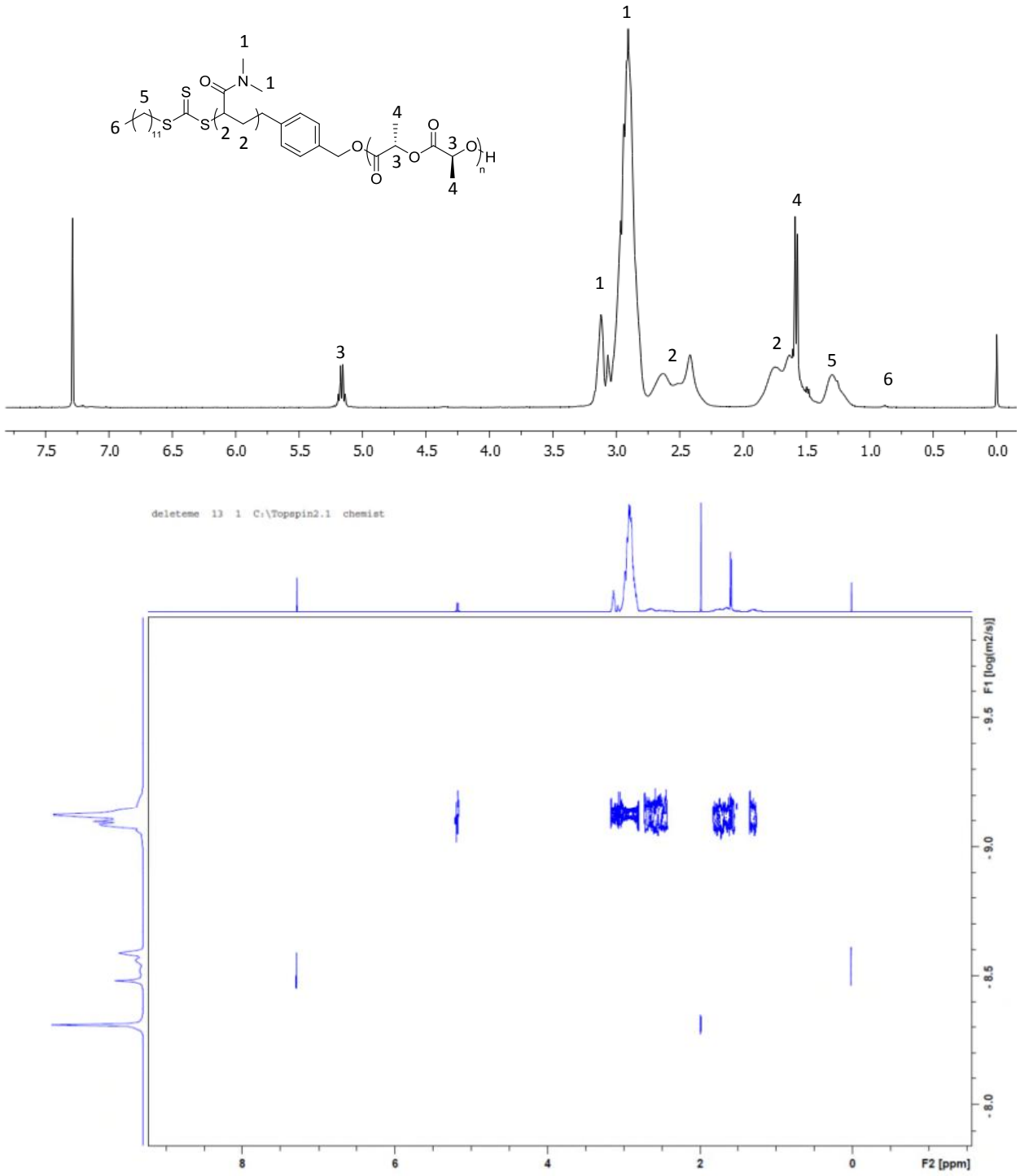

Figure S1. ^{1}H NMR spectrum (top) and DOSY (bottom) (400 MHz, $CDCl_3$) of PDMA-*b*-PLLA.

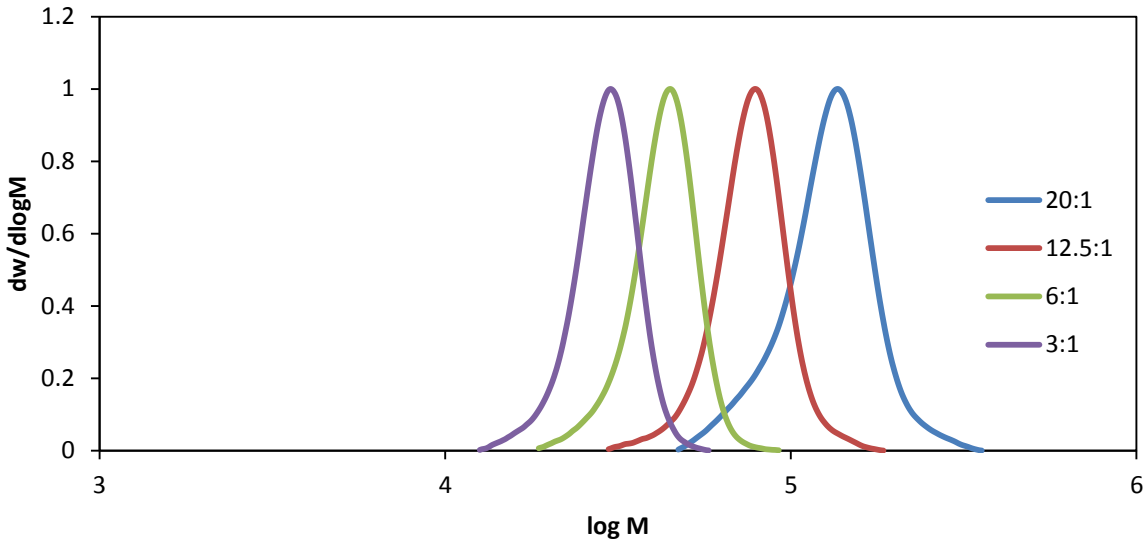

Figure S2. Overlaid refractive index and ultraviolet (λ = 309 nm) SEC chromatograms for PDMA-*b*-PLLA$_{48}$ diblock copolymers of corona-core ratios 20:1 ($Đ_M$ = 1.10), 12.5:1 ($Đ_M$ = 1.06), 5:1($Đ_M$ = 1.05) and 3:1 ($Đ_M$ = 1.05).

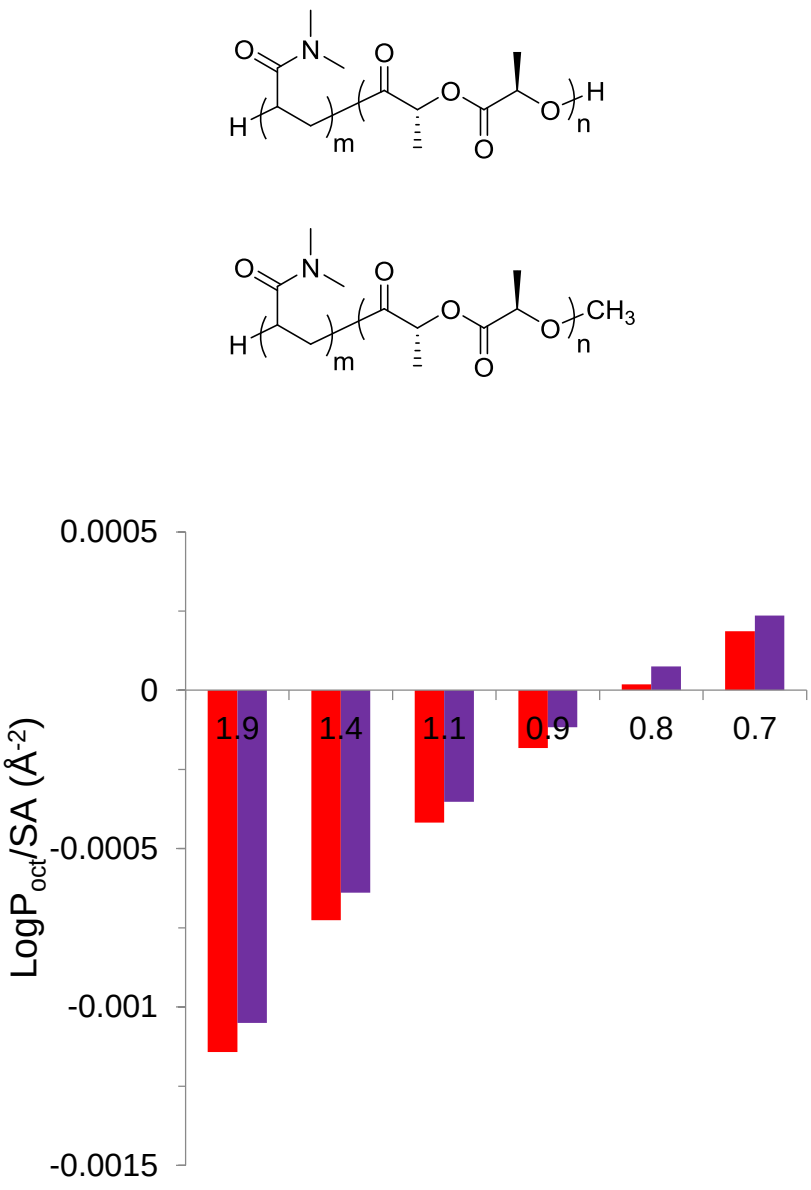

Figure S3. Octanol-water partition coefficients (*LogP*$_{oct}$) normalized by surface area (SA) (bottom) for PDMA-*b*-PLLA diblock copolymers (top). The x-axis shows the ratio of DMA:lactide units in the PDMA-*b*-PLLA diblock copolymer with OH endgroup (red columns) and MeO endgroup (purple columns). All the molecular models contained a constant number of DMA units (21) with varying numbers of lactide units. Calculations performed with Materials Studio after Forcite geometry optimization of diblock copolymers using a 1.4 Å probe for the Connolly SA calculation

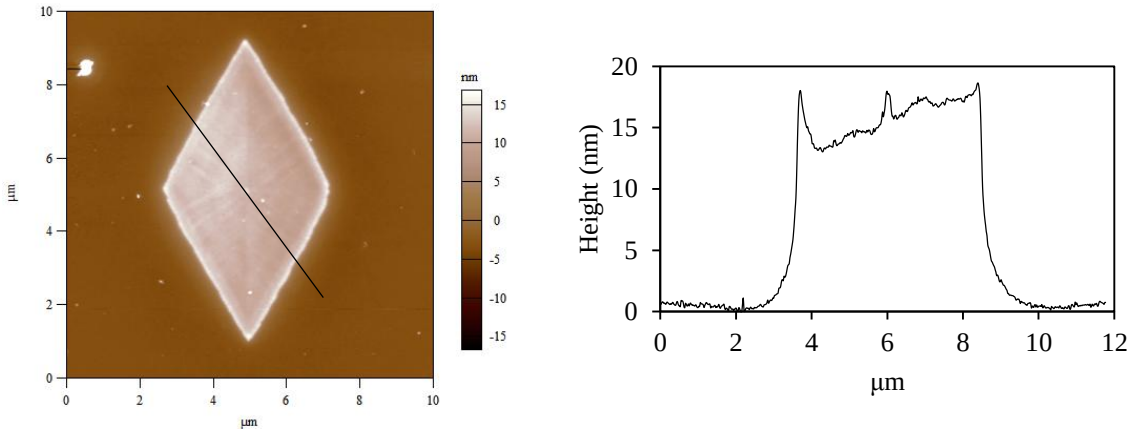

Figure S4. AFM and height profile of 20:1 $PDMA_{1000}$-*b*-$PLLA_{48}$ diamond platelet. Samples were self-assembled in ethanol at 90 °C for 8 h with subsequent slow cooling.

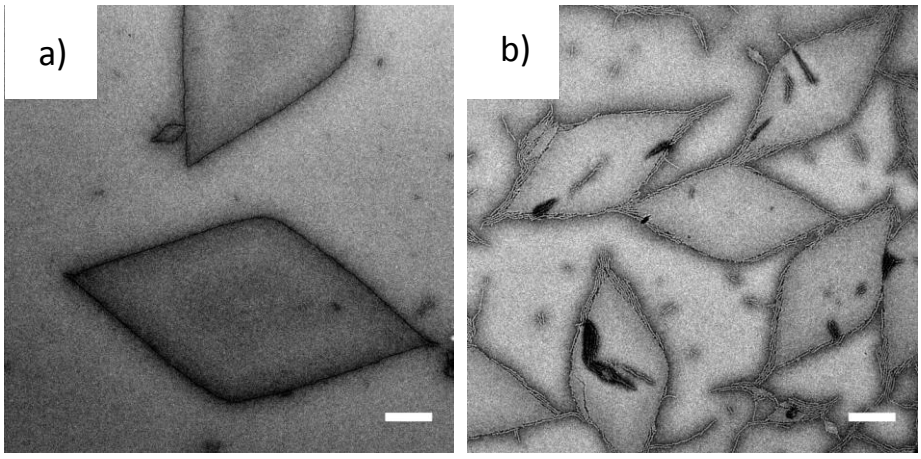

Figure S5. TEM micrographs of PDMA-*b*-$PLLA_{48}$ block copolymers of corona-core ratios of (a) 5:1, and (b) 3:1. Samples were self-assembled in ethanol at 90 °C for 18 h and cooled to room temperature. All samples were stained with uranyl acetate. Scale bar = 1 µm.

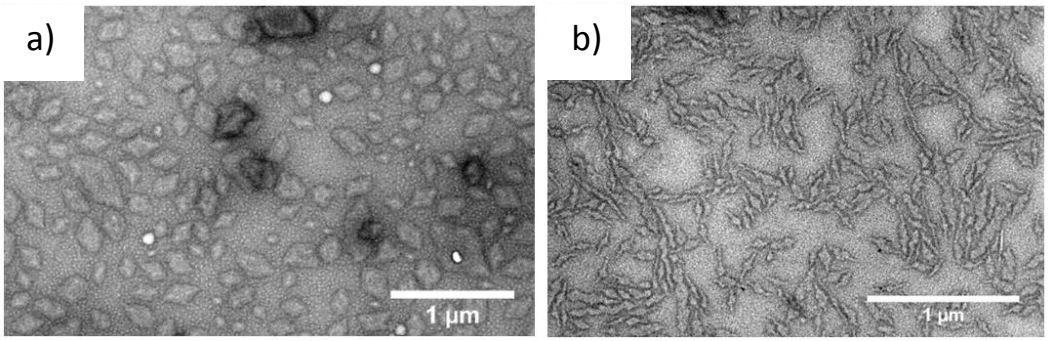

Figure S6. TEM micrographs of a series of PDMA-*b*-PLLA$_{25}$ block copolymers of corona-core ratios of (a) 10:1, (b) 5:1. Samples were self-assembled in ethanol at 65 °C for 18 h and cooled to room temperature. All samples were stained with uranyl acetate. Scale bar = 1 µm.

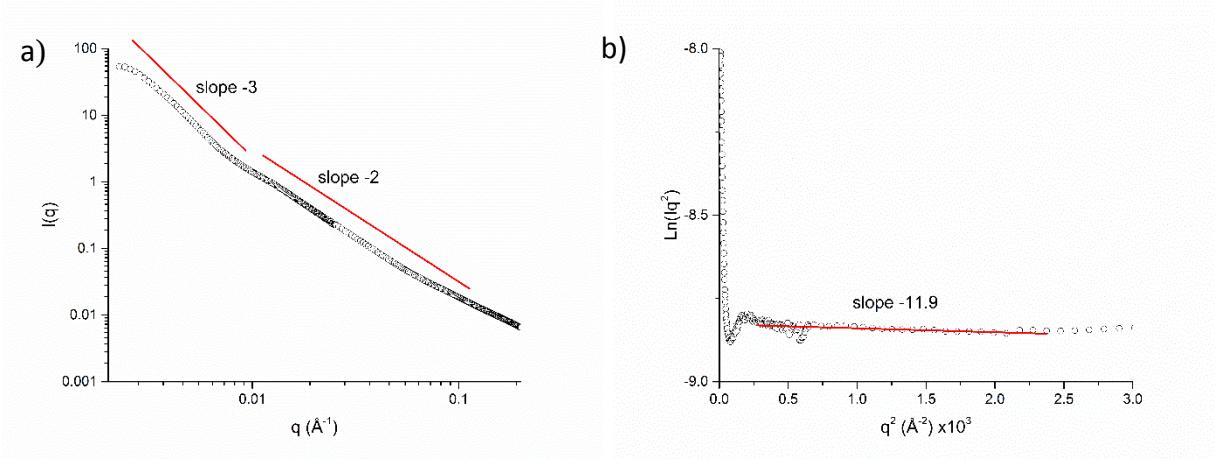

Figure S7. (a) Small-angle X-ray scattering profile for PDMA$_{1000}$-*b*-PLLA$_{48}$ (20:1 corona-core ratio) self-assembled at 65 °C in ethanol and (b) Guinier plot for platelet objects.

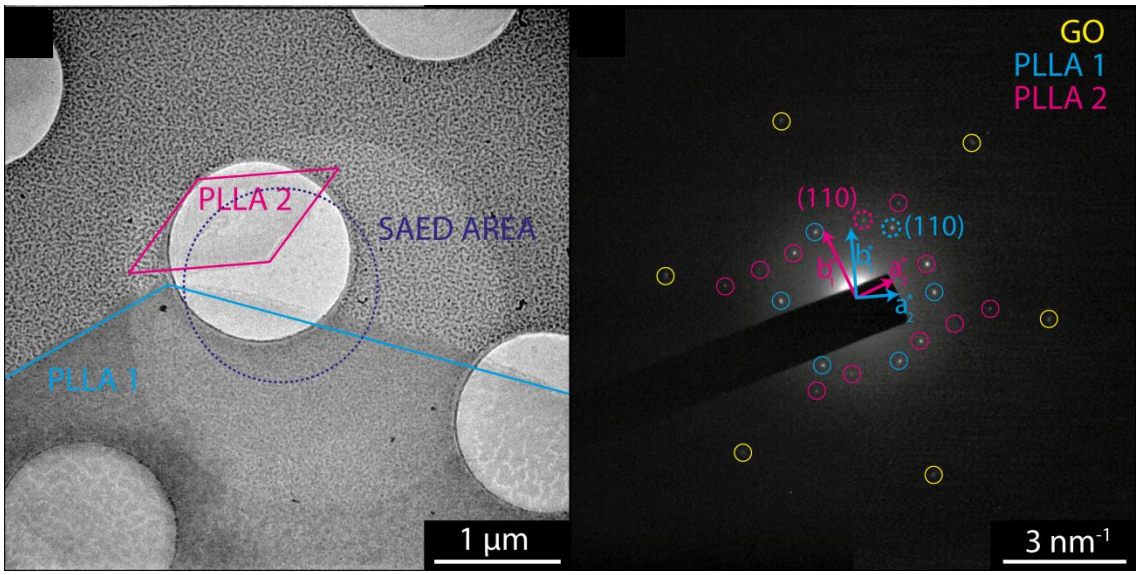

Figure S8. SAED analysis of $PDMA_{1000}$-*b*-$PLLA_{48}$ (20:1 corona-core ratio) diamond platelets.

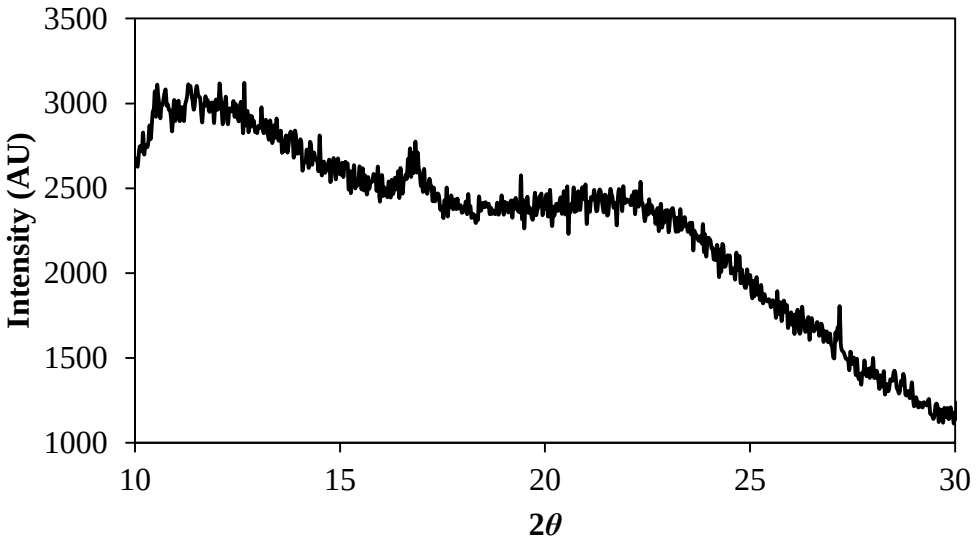

Figure S9. WAXS diffractogram of $PDMA_{1000}$-*b*-$PLLA_{48}$ (20:1 corona-core ratio) diamond platelets showing the 2θ peak at 16° characteristic of crystalline PLLA. The broad background signal is attributable to the amorphous large PDMA block for this block copolymer (20:1).

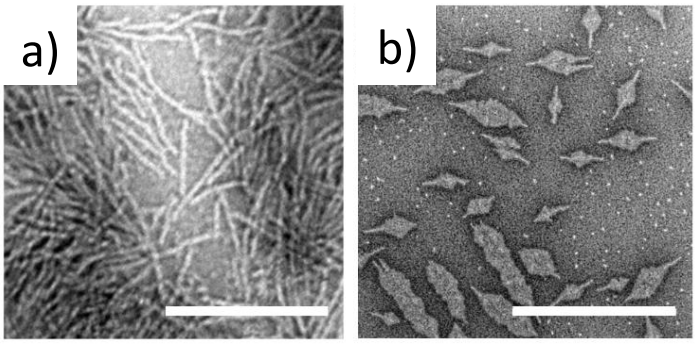

Figure S10. TEM micrographs of cylinder-forming (corona-core ratio 3:1) $PDMA_{150}$-*b*-$PLLA_{48}$ block copolymers (a) unmodified and (b) modified with a carboxylic acid group. Samples were self-assembled in ethanol at 90 °C for 8 h with and cooled to room temperature. Samples were stained with uranyl acetate. Scale bar = 1 µm.

a)

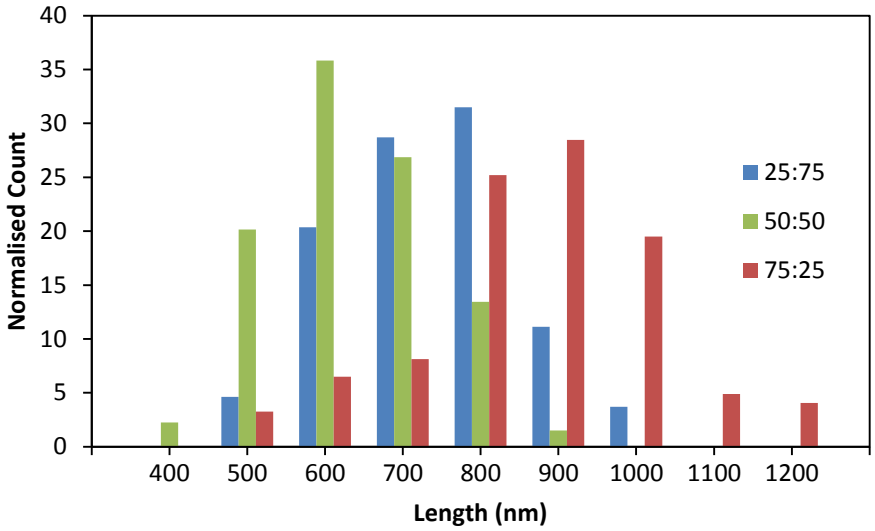

b)

Blending Ratio	L_w[a] (nm)	L_n[a] (nm)	L_w/L_n
25:75	754	735	1.03
50:50	734	695	1.06
75:25	965	912	1.06

[a] As determined by TEM analysis, see Materials and Methods section for details

Figure S11. (a) Histograms and (b) characterization data showing the length distribution of attached cylindrical micelles within hierarchical structures (prepared *via* PDMA-b-PLLA$_{48}$ blends of block ratios 20:1 and 3:1, at blending ratios of 25:75, 50:50 and 75:25, self-assembled in ethanol at 90 °C for 8 h and cooled to room temperature).

References

1 B. G. Lohmeijer, R. C. Pratt, F. Leibfarth, J. W. Logan, D. A. Long, A. P. Dove, F. Nederberg, J. Choi, C. Wade and R. M. Waymouth, *Macromolecules*, 2006, **39**, 8574-8583.

2 J. Skey and R. K. O'Reilly, *Chem. Commun.*, 2008, 4183-4185.

3 N. Petzetakis, A. P. Dove and R. K. O'Reilly, *Chem. Sci.*, 2011, **2**, 955-960.

4 A. Pitto-Barry, N. Kirby, A. P. Dove and R. K. O'Reilly, *Polym. Chem.*, 2014, **5**, 1427-1436.

5 J. P. Patterson, A. M. Sanchez, N. Petzetakis, T. P. Smart, T. H. Epps III, I. Portman, N. R. Wilson and R. K. O'Reilly, *Soft Matter*, 2012, **8**, 3322-3328.